Chapter 2
Physical Properties of Fibres and Matrix

2.1 Introduction

The previous chapter described how the fibre thickness and length play an important role in directing the fracture stress of the fibre from an atomic perspective. The purpose of this chapter was to indicate the basic concepts related to the physical properties of the fibres and matrix at the fibre length scale and how these properties connect to the bulk properties of the DFRC. These properties are grouped under two categories, namely structure and material properties. In this book, the basic concepts related to the structure of a DFRC are concerned with fibre slenderness and shape, fibre–fibre separation and fibre orientation. The basic concepts related to the material properties are concerned with modulus of elasticity, fracture strength, strain energy density to resilience and rupture, and the probabilistic sense of fracture strength.

The discussion in this chapter is organized as follows. To begin, Sect. 2.2 provides an overview of the response of a DFRC to an external load, from initial loading until the composite ruptures. With regards to fibre structure, Sect. 2.3.1 provides a general description of the fibre shape, size and arrangement in a DFRC; the information in this section will lend to the arguments for establishing the models of stress transfer and fracture. The description of fibre size is further elaborated with regards to the fibre aspect ratio in Sect. 2.3.2. The significance of the DFRC structural composition for load-sharing is explained in Sect. 2.3.3. The influence of fibre orientation on the mechanical properties of a DFRC and the significance of fibre packing configuration are explained in Sects. 2.3.4 and 2.3.5, respectively. Next, the subject of fibre and matrix material properties are discussed with reference to (1) the rule of mixture for modelling the composite stiffness (Sect. 2.4.1) and strength (Sect. 2.4.2), (2) how fibre size directs the resilience and fracture energy of the DFRC, and (3) the concept of probabilistic analysis for fracture strength.

K.L. Goh, *Discontinuous-Fibre Reinforced Composites*, Engineering Materials and Processes, DOI 10.1007/978-1-4471-7305-2_2

2.2 Composite Stress–Strain Profiles

The response of the DFRC to an external applied load may be described by the stress versus strain data. The stress–strain behaviour of a DFRC provides the basis for many of the arguments presented in this book. Here, this section presents the key aspects of stress versus strain curves of DFRC and how the different regions on the curves correspond to the respective reinforcement mechanisms.

Consider strong, stiff and short fibres, aligned and uniformly dispersed in a weak and soft matrix. The fibre interacts with the matrix through either mechanical or chemical coupling at the fibre–matrix interface (Sect. 1.5). An external tensile load, of increasing magnitude, is applied on the composite; the load acts in the direction of the fibres. Owing to the difference in the elastic modulus between the matrix and fibre materials, this generates an interfacial stress which is responsible for the mechanism of stress transfer. The fibre–matrix interaction at the interface underpins the stress transfer mechanism; the nature of the interaction determines both the rigidity of the composite and the resistance of the composite to rupture [9, 20].

Figure 2.1 shows the stress–strain curves of a hypothetical DFRC at varying fibre volume fraction, V_f. Here, V_f is defined as the ratio of the volume of the fibres to the volume of the composite material. Consequently, the volume fraction of the matrix, $V_m = 1 - V_f$. The $V_f = 100$ % represents an all-fibre material and $V_f = 0$ represents an all-matrix material. The all-fibre material (blue curve, $V_f = 100$ %) is stiffest and strongest. However, brittle fibres (solid lines) are expected to break,

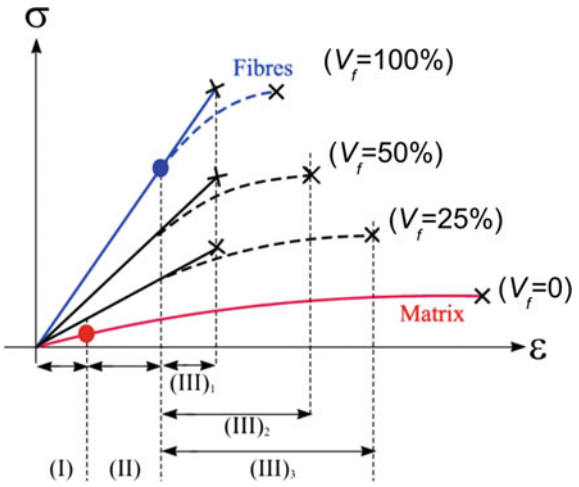

Fig. 2.1 Graph of composite stress, σ, versus composite strain, ε, for different composition of fibre and matrix materials (1). Here, *times symbol* represents fracture points. *Roman numerals* (I), (II) and (III) refer to elastic load transfer, plastic load transfer and plastic composite, respectively [1, 2, 21]; *subscript 1* denotes the case of brittle fibres while *2* and *3* denotes the case of ductile fibres. *Dotted* and *solid lines* represent ductile and brittle fibres, respectively

at their maximum stress, at a lower strain as compared to ductile fibres (dashes). The all-matrix material (V_f = 0 %) is the softest and weakest. The composites at V_f = 50 % and = 25 % show gradients and maximum stress lying in between the cases of all-fibre (V_f = 100 %) and all-matrix (V_f = 0 %) materials.

The stress–strain curves corresponding to the composite materials may be divided into three regions, namely I, II and III, according to different mechanisms of reinforcement [1, 2, 21]. Thus, region I, II and III correspond to elastic stress transfer [30, 72–75], plastic stress transfer [14–15, 73] including plastic composite [73], respectively. The vertical dashes are used to demarcate these regions. If the composite is highly brittle, the response of the composite produces a linear stress versus strain relationship from initial loading until rupture [21]; a ductile composite responds nonlinearly until it ruptures. Thus, the response of the composite comprises a series of mechanisms that regulate the stress transfer process from initial loading until the composite ruptures [73].

In addition, intermediate modes, such as mode α (matrix yielding), γ (matrix cracking) and β (interfacial debonding), occur in transition from elastic to plastic stress transfer [73]. In the final stage leading up to composite rupture, a series of events is expected to occur namely, fibre pull-out [73, 77], matrix rupture and fibre rupture [73, 76]. Further details concerning these mechanisms of stress transfer and fracture are discussed in Chaps. 3–6.

2.3 Structure

2.3.1 General Descriptions of Fibre Shape, Size and Arrangement

In this book, both fibre and matrix materials will always be considered to be homogeneous and isotropic. Unless otherwise stated, the fibre possesses a uniform cylinder (Fig. 2.2), which is widely used in DFRCs. Of note, discontinuous fibres need not be uniform cylindrical in shape (Sect. 1.7); they could be ellipsoidal, with paraboloidal ends or straight tapered ends [6–7, 17–19, 78]. Fibres also need not be cylindrical in cross section; fibres which have non-cylindrical cross sections, such as star-shaped cross sections, have been investigated [22]. For simplicity, in this book the focus is on fibres with cylindrical cross sections.

Figure 2.2 illustrates the axis-symmetry and mirror-symmetry feature of the fibre. Here, the fibre centre defines the origin of a cylindrical polar coordinate system. The fibre axis defines the z-axis of the system. Here, (r, ϕ, z) will be used to represent the ordinates of the cylindrical polar coordinate system. For simplicity, the models of the discontinuous fibres reinforcing the composite material will always be considered to be axisymmetric and mirror symmetric about the fibre centre. Owing to mirror symmetry about the fibre centre, the discussion presented in this book is merely concerned with one half of the fibre, unless otherwise stated.

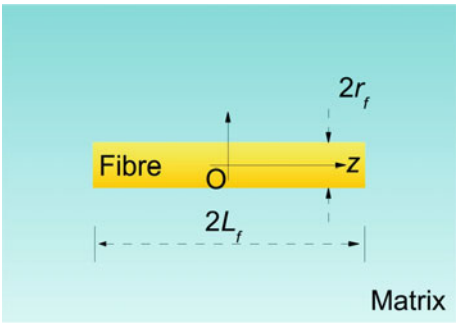

Fig. 2.2 A uniform cylindrical fibre embedded in a matrix material. The fibre diameter and length are $2r_f$ and $2L_f$, respectively. The centre of the fibre defines the origin, O, of the cylindrical polar coordinate system; here, z-axis is aligned in the direction of the fibre axis

With reference to Fig. 2.2, let L_f be the half-length of the fibre. The fibre has a radius, r_f, which can vary along the length. For the purpose of generalizing to fibres of non-uniform shapes, such as fibre with tapering ends, the symbol r_o will be used to refer to the radius of the fibre at O; this corresponds to a diameter of D_f (= $2r_o$). In this book, where uniform cylindrical fibres are concerned, r_f (or r_o) can be used interchangeably to refer to the fibre radius without loss of ambiguity.

In this book the fibres are always arranged in a unidirectional manner [23]. As shown in Fig. 1.2c, in the transverse plane, the spacing between fibres may not be identical; along the longitudinal direction, the axial spacing need not also be identical. Without loss of generality, at the microscopic level, bundles of fibres may also exhibit regular lateral arrangement, such as square-diagonal packing, square-edge packing or triangular-edge packing (a.k.a. hexagonal packing). However, the number of fibres present in the DFRC is always sufficiently large for the arrangement to be considered to be fairly uniformly distributed, at bulk level. Let A_f be the cross-sectional area of a fibre and A_c the cross-sectional area of the DFRC (i.e. normal to the fibre axis). Let N be the number of fibres present within a cross section of the DFRC. In this way, the fibre area fraction, defined as the ratio of NA_f to A_c, is a constant at any given cross-sectional plane of the DFRC [23].

The applied load acting on the DFRC acts in the direction of the fibre axis—this action deforms the matrix material [14, 15]. At the fibre–matrix interface, the contact between the fibre and the matrix results in a τ [14, 15]. Consequently, this induces stresses within the fibre [14, 15]. Since the external tensile load is applied in the direction parallel to the fibre axis, the mechanical response of the fibre is of an axisymmetric nature [14, 15]. Thus, the τ and the induced σ_z and σ_r within the fibre are independent of ϕ [14, 15].

2.3.2 *Fibre Aspect Ratio*

Fibre sizes may be referred to by their lengths and thicknesses (diameters or radii), but a more convenient size parameter is the fibre aspect ratio (q). The q is defined as

$$q = L_f / r_o. \tag{2.1}$$

Thus, the q is a normalized dimensionless quantity which may be used to describe the fibre slenderness [24]. Although one could envisage that thick fibres would yield composite with high strength, the fibres could be thick but stubby (i.e. short) and hence would not facilitate high stress uptake. Conversely, although one could envisage that thin fibres would yield composite with low strength, but these fibres could be thin and long and hence would promote high stress uptake. Thus, the q is a useful quantity (than L_f or r_f) because it incorporates both thickness and length.

The q plays an important role in influencing the stiffness, yield and fracture strengths, yield and fracture strains and the resilience and fracture toughness of a DFRC. Figure 2.3a shows the copper–tungsten fibre composite stress–strain results reported by Kelly and Tyson [5]. The stress–strain plot reveals that specimens of different qs share a common feature, i.e. a fairly linear elastic region over a large proportion between initial loading and yield strain (Y). Thereafter, the region of plasticity (beyond the yield point) appears to increase with increase in q. Figure 2.3b–h shows graphs of the respective mechanical properties of the copper–tungsten fibre composite, namely the elastic modulus (E), yield strength (σ_Y), fracture strength (σ_U), yield strain (ε_Y), strain to rupture (ε_U), strain energy density for resilience (u_Y) and strain energy density to fracture (u_C), versus q. The E is identified with the gradient of the linear region of the stress–strain curve shown in Fig. 2.3a. The u_Y and u_C (a.k.a. fracture toughness in this book) are identified with the respective areas under the curve from the point of initial loading up to the yield point and the maximum strain. According to the results shown in Fig. 2.3b–h, it can be concluded that the magnitudes of the respective mechanical properties increase with increasing q.

Some further insights may be derived from these results:

- To some extent, q has a dramatic effect on E; E changes from 1600 to 2000 k.s.i as q increases from 5 to 40. This study shows that mechanical adhesion at the fibre–matrix interface enables tungsten fibres to provide reinforcement to the copper matrix. If chemical bonding were present at the fibre–matrix interface, E could increase more dramatically with q, over the same range of values.
- The σ_U and u_C relate to two different fracture mechanisms. The mechanism involves in σ_U addresses the load-sharing concept which is explained in Sect. 2.3.3. With regards to u_C, at the microscopic level, u_C refers to the extent (or depth) of the mechanical disturbance into the composite fine structure during the fracture process. Since the frictional force and work done to overcome friction at the fibre–matrix interface remain the same (because there is no change in the material properties), it can only mean that a high u_C reflects a greater extent of disturbance throughout the interface. In the presence of higher q (-particularly with longer fibres), the energy needed to cause sliding throughout the interface increases. Thus, one finds u_C increases with q at the macroscopic level. When fibres with larger q (i.e. greater than the critical q) rupture, this

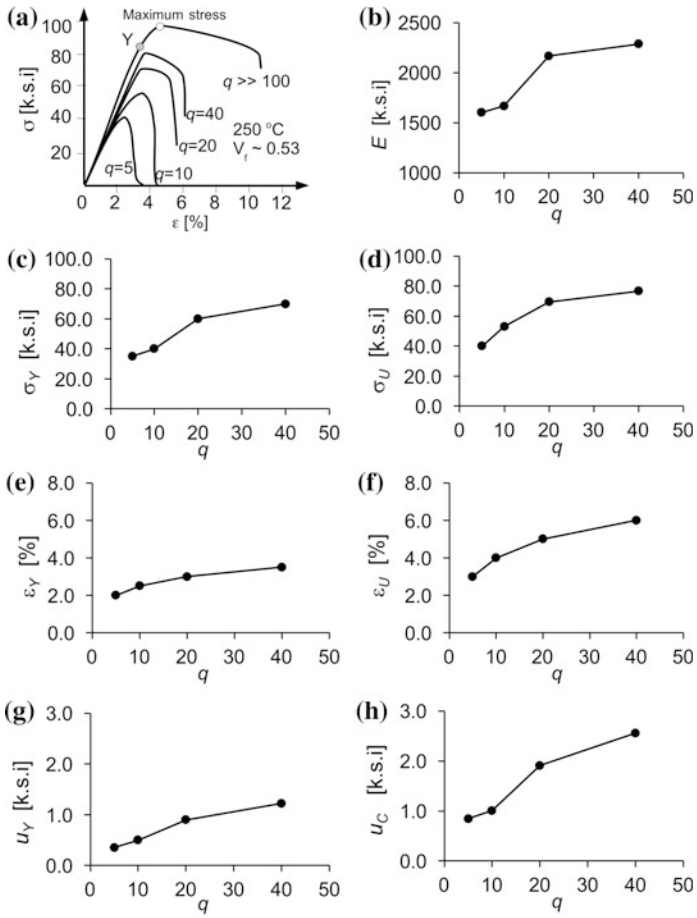

Fig. 2.3 Mechanical properties of fibre reinforced composites. **a** Graph of composite stress (σ) versus composite strain (ε) for tungsten fibres reinforcing copper composite material with varying fibre aspect ratio, q. Graphs of the composite **b** elastic modulus (E, a.k.a. stiffness), **c** tensile yield strength (σ_Y), **d** tensile fracture strength (σ_U), **e** yield strain (ε_Y), **f** strain to rupture (ε_U), **g** the resilience strain energy density (u_Y) and **h** the strain energy density to fracture (u_C), versus q. Adapted from Kelly and Tyson (5). In part A, symbol Y denotes the yield point (indicated by a *circle* on the stress–strain curve). 1 k.s.i. $\approx$ 6.9 MPa

results in fragments with smaller q but they could still cope with maximal stress uptake if they satisfy the critical q; in other words, the qs are larger than the critical q (Sect. 6.2.3). Subsequent fragmentation could produce fibre fragments with qs smaller than the critical q [16]. These fibres take up stresses with lower magnitude because they possess lower q; they will also not fracture because the stress taken up in these fibres will not reach the fracture strength of the fibre. Further details concerning the fracture of fibres can be found in Sect. 6.2.3.

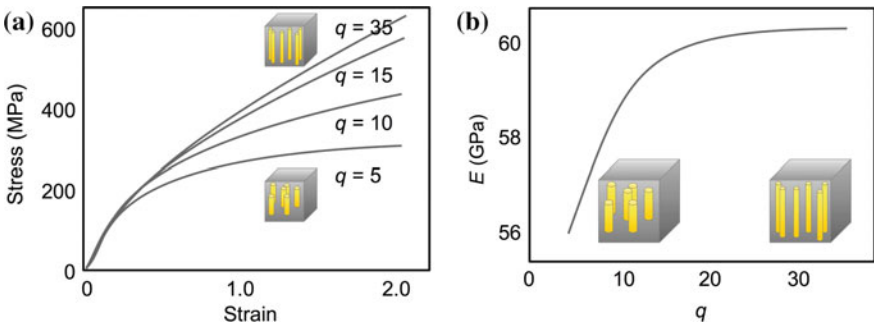

Fig. 2.4 Effects of fibre aspect ratio (q) on the composite mechanical properties. **a** Graph of stress versus strain, for varying fibre aspect ratio (q). **b** Composite stiffness, E, versus q. The results are derived from finite element analysis of three-dimensional representative volume element models (67)

The results of Kelly and Tyson [5] have been compared with predictions from finite element (FE) analysis of three-dimensional representative volume element (RVE) models of DFRCs for discontinuous carbon fibres reinforcing magnesium matrix material [25]. Of note, the concept of a RVE is similar to the unit cell concept used in crystal structure analysis; the RVE refers to the smallest unit of volume that contains all of the structural and symmetry information necessary to build up the macroscopic structure of the DFRC. The predictions derived from the RVE models reveal that the profiles of the stress–strain curves converge at high q values (Fig 2.4a) [25]. The predictions from these models also reveal that the E increases with increasing q (in particular, the E may plateau out at large q as shown in Fig. 2.4b) [25, 26]. The general trends in these predictions of the composite stress–strain curves and in the plot of E for varying q values are in good agreement with those reported by Kelly and Tyson [5].

2.3.3 *How Structure Accounts for Load-Sharing in Composites*

The term 'load-sharing' is often invoked in the discussion of fibre reinforced composites [4, 27, 28]. This term is used to account for how the fibres and matrix 'share' the total load acting on the composite [4, 27, 28]. How does the structure of the DFRC influence the load-sharing capacity? For simplicity, consider a RVE of the DFRC shown in Fig. 2.5a. The composite material is acted upon by an increasing external tensile load applied in the direction of the fibre axis. The dimensions of the RVE are indicated by Δx, Δy and Δz which represent the respective length, width and height of the volume element; these also correspond to the direction of the x, y and z axes of the Cartesian coordinate system. The cross-sectional area of the RVE, normal to the fibre axis, is given by

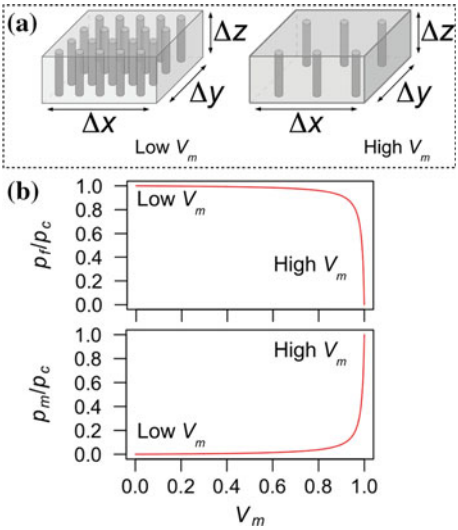

Fig. 2.5 Effects of matrix volume fraction on the loads in the fibres and matrix in the DFRC. **a** Schematics of a rectangular representative volume element (RVE) of the composite material, where Δx, Δy and Δz represents the respective length, width and height of the element (corresponding to the direction of the x, y and z axes of the Cartesian coordinate system), to illustrate the low and high matrix volume fraction, V_m. Here, the term RVE refers to the smallest unit of volume in the DFRC that contains all of the fibre structural and symmetry information necessary to build up the macroscopic structure of the DFRC. **b** *Top panel* graph of the dimensionless fibre load, p_f/p_c, versus V_m; *bottom panel* graph of the dimensionless matrix load, p_m/p_c, versus V_m. These graphs were derived using the analytical (load-sharing) model given by Eqs. (2.10) and (2.11). Symbol p_c denotes the load on the composite

$$A_c = \Delta x \Delta y, \tag{2.2}$$

and $\Delta z = 2L_f$.

For a composite system containing fibres and matrix, one finds

$$V_f + V_m = 1. \tag{2.3}$$

By assuming that the fibres are arranged as shown in Fig. 1.2c, and invoking the assumptions of constant area fractions of the fibre (see Sect. 2.3.1), one may be able to estimate the V_f and V_m (see Eq. 2.3) by noting that $V_f = NA_f\Delta z/\{A_c\Delta z\}$ and $V_m = A_m\Delta z/\{A_c\Delta z\} = (A_c - NA_f)\Delta z/\{A_c\Delta z\}$, where A_f and A_m are the respective cross-sectional areas of the matrix and a fibre, and $A_c = NA_f + A_m$. This results in

$$\begin{aligned} V_f &= NA_f/A_c, \\ V_m &= 1 - V_f. \end{aligned} \tag{2.4}$$

Provided that the fibres and matrix within the RVE undergo a constant uniform deformation, this deformation is the result of a normal stress (with an average value σ) acting on the area A_c. Let $\langle\sigma_z\rangle$ and σ_m represent the average normal stresses in the fibre and the matrix, respectively; $\langle\sigma_z\rangle$ and σ_m act, i.e. perpendicularly, to the respective fibre and matrix cross sections. The fibres and matrix within the element are subjected to the respective forces which may be estimated to order of magnitude by

$$p_f = \langle\sigma_z\rangle N A_f, \tag{2.5}$$

$$p_m = \sigma_m A_m, \tag{2.6}$$

where A_m is the cross-sectional area of the matrix. The force acting over A_c is given by

$$p_c = \sigma A_c. \tag{2.7}$$

Applying the force equilibrium argument for the system of fibres embedded in the matrix element, the sum of these forces, i.e. p_f and p_m, acting over A_c must be equivalent to the force p_c acting perpendicularly to A_c, i.e.

$$p_c = p_m + p_f \tag{2.8}$$

[23]. By the condition of compatibility of displacement, i.e. $p_m\Delta_z/\{[A_c - NA_f]E_m\} = p_f\Delta_z/\{NA_fE_f\}$, this leads to a second equation relating p_f and p_m,

$$p_m/\{V_mE_m\} = p_f/\{V_fE_f\}. \tag{2.9}$$

Evaluating the equations for the force equilibrium (Eq. 2.8) and compatibility of displacement (Eq. 2.9) leads to three simple expressions,

$$p_f = p_cV_fE_f/E, \tag{2.10}$$

$$p_m = p_cV_mE_m/E, \tag{2.11}$$

and

$$E = E_fV_f + E_mV_m, \tag{2.12}$$

[23]. Equation (2.12) is known as the rule of mixture for the composite stiffness; this shall be elaborated further in Sect. 2.4.1. More importantly, in this discussion on the load-sharing issue, Eqs. (2.10) and (2.11) describe the forces in the fibre and the matrix for the analytical (load-sharing) model. Of note, since the volumes of the fibre and matrix affect the forces through E, the main concern here is the sensitivity of these forces to the variation in the volumes of the fibre and matrix, in addition to the dependence on the respective ratio of the elastic moduli of the fibre and matrix to the composite stiffness.

For the purpose of illustration, Fig. 2.5b shows a graph of the dimensionless forces in the fibres (p_f/p_c) and matrix (p_m/p_c) versus V_m, for $E_f = 1 \times 10^9$ Pa and $E_m = 1 \times 10^7$ Pa. Thus, the magnitude of the normalized force in the fibres decreases nonlinearly as V_m increases; in particular, the slope of the decrease is very steep at large V_m. In other words, as the matrix volume increases, the load taken up by the fibres decreases but the load taken up by the matrix increases. To conclude, these arguments highlight that the load sharing capability of a DFRC depends not only on the mechanical properties of the fibre and matrix (i.e. the stiffness of the fibre and matrix), but also on the volumes of the fibres and matrix. To sum up the discussion, this is how structure of the DFRC affects the load-sharing capacity.

2.3.4 *Fibre Orientation*

Consider a tensile force applied to the DFRC at an angle, θ, with respect to the fibre-axis direction (Fig. 2.6). The restoring stress in the fibres, and so their ability to balance the applied stress, would be reduced by a factor of $[\cos(\theta)]^4$. In this case, the efficiency of reinforcement, η, will be of the order of $[\cos(\theta)]^4$ [2]. The orientation of the fibres within the matrix is expected to regulate the material properties of the composite. A DFRC intended for sustaining tensile load would require that the fibres be arranged in the direction of the applied load. On the other hand, a DFRC containing randomly oriented fibres is expected to be able to sustain load better in compression than in tension.

Mortazavian and Fatemi [29] have applied a simple model to describe the influence of fibre orientation on the stiffness and fracture strength of a DFRC. Let E_L and E_T be the elastic moduli of the DFRC corresponding to two cases known as, respectively, the longitudinal and transverse directions (these refer to the orientation of the aligned fibres with respect to the direction of the external applied load). Let

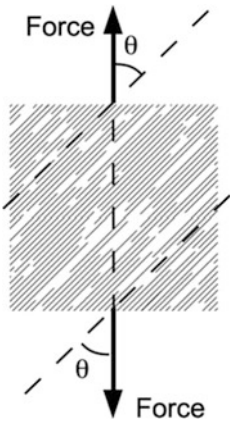

Fig. 2.6 An external force acting obliquely (at angle θ) with respect to the direction of the fibres in a DFRC

G and v denote the shear modulus and Poisson's ratio of the DFRC; these are assumed to be independent of the direction of loading with respect to the fibre orientation direction. Mortazavian and Fatemi [29] proposed that the stiffness of the DFRC may be expression as a function of θ, i.e.

$$E = \{\cos(\theta)^4/E_L + \sin(\theta)^4/E_T + [1/4]\{1/G - 2v/E_L\}\sin(2\theta)^2\}^{-1}. \quad (2.13)$$

The equation that describes the influence of fibre orientation on the fracture strength of a DFRC is given by [29],

$$\sigma_U = \{\cos(\theta)^4/\sigma_L^2 + \sin(\theta)^4/\sigma_T^2 + \{1/t^2 - 1/\sigma_L^2\}\sin(\theta)^2\cos(\theta)^2\}^{-1/2}, \quad (2.14)$$

where σ_U is identified as a function of θ, σ_L and σ_T are the strength of the composite corresponding to, respectively, the longitudinal and transverse directions, and the τ is used here to represent the fibre–matrix interfacial shear stress that results in a disruption to the adhesion between the fibre and the matrix [29].

For the purpose of illustration, Fig. 2.7 shows a plot of E versus θ and $_U$ versus θ for a DFRC. The values of E_L, E_T, σ_L , σ_T, v, G and τ_U used for deriving the plots are explained in the figure caption. Of note, it is reasonable to expect that $E_L > E_T$ and $\sigma_L > \sigma_T$. For both curves, the maximum E and σ_U occur at $\theta = 0$, as well as at 180°. From the maximum E, the E and σ_U decrease with increase in θ until 90°; thereafter the E and σ_U increase with increase in θ until 180°.

Tian and coworkers has developed a RVE model of a DFRC to study fibre orientation effects by finite element (FE) analysis [25]. Predictions of the stress versus strain response of the RVE (Fig. 2.8a) revealed that the fracture strength (which is identified as the maximum stress on the stress versus strain curve) decreases with increasing θ, from 0° to 60°. Thereafter, the fracture strength appears to converge somewhat, as the θ approaches 90° (Fig. 2.8b). Remarkably, the trends in these predictions are in good agreement with those determined by the analytical model proposed by Mortazavian and Fatemi [29].

For simplicity, hereafter the discussion in this book will address only the case of $\theta = 0$, consequently $E = E_L$ and $\sigma_U = \sigma_L$. While this is a special case of θ, it may be argued that when θ is not zero, increasing the load may cause these fibres to realign towards the direction of the load. Henceforth, these cases may be regarded as equivalent to $\theta = 0$.

2.3.5 *Fibre Packing Distribution*

It is shown that the mechanical properties of the composite, such as stiffness (Sect. 2.4.1), are related to V_f. However, it could be that the mechanical properties and V_f are both related to a third variable, namely the fibre–fibre separation distance, ρ. The ρ is expected to vary depending on the fibre packing configuration. In

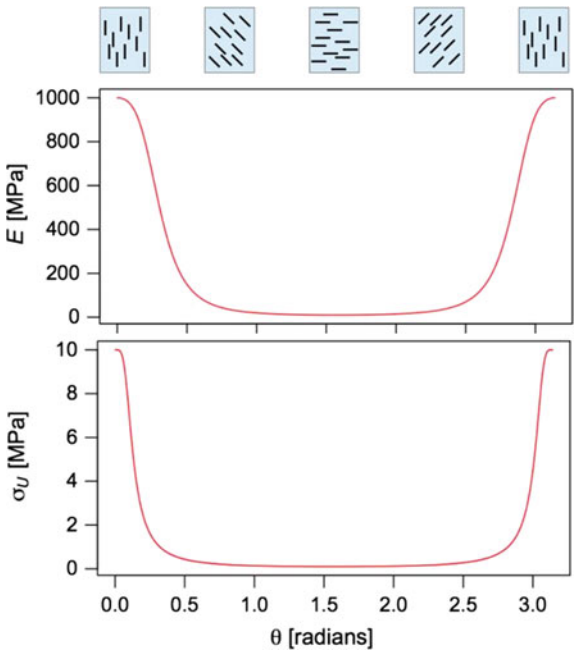

Fig. 2.7 Graphs of the stiffness, E, and fracture strength, σ_U, of a DFRC versus the orientation angle, θ. Insets show the discontinuous fibres embedded in the matrix, at various orientation angle; the applied load is acting vertically on the DFRC. Here, the E and σ_U versus θ was evaluated using Eqs. (2.13) and (2.14), respectively, where the longitudinal stiffness, E_L = 1 GPa, the transverse stiffness, E_T = 10 MPa, the longitudinal fracture strength, σ_L = 10 MPa, the transverse fracture strength, σ_T = 0.1 MPa, and Poisson's ratio of the DFRC ν = 0.3. Without loss of generality, for this numerical illustration, it is assumed that the interfacial shear stress τ is of order of the DFRC shear modulus (G) and $G = \{(E_L + E_T)/2\}/(2 + 2\nu)$, where $(E_L + E_T)/2$ represents the 'effective stiffness' of the DFRC

this section, simple arguments are presented to relate V_f to ρ. For simplicity, let ρ describes the centre-to-centre distance between adjacent fibres. For discontinuous fibres, one invokes two assumptions: (1) that there is a sufficiently large number of fibres, such that at the microscopic length scale, the lateral arrangement appears somewhat regular (as indicated previously in Sect. 2.3.1), e.g. different bundles of the fibres are arranged laterally in the square packing configuration (Fig. 2.9b) and (2) that, longitudinally, most fibres would be lined with ends very close to the next fibre. Note that for the square packing configuration, the region abcd (area = ρ^2) defined in Fig. 2.9b encloses one fibre; the cross-sectional area of the fibre is given by πr_f^2. Thus, V_f is given by $V_f = \{\pi r_f^2\}L_f/[\rho^2 L_f]$ which simplifies to [30, 71]

$$V_f = \pi r_f^2/\rho^2. \tag{2.15}$$

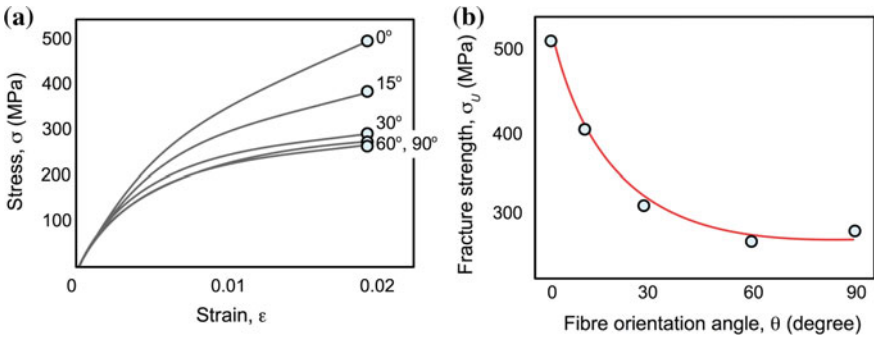

Fig. 2.8 Graphs of the **a** stress (σ) versus strain (ε) for varying fibre orientation angle, θ, and **b** fracture strength, σ_U, versus fibre orientation angle, θ, of discontinuous carbon fibres reinforced magnesium composites. These plots are derived from finite element analysis of a representative volume element of the DFRC [25]. Symmetry (see Fig. 2.7b) dictates that only the effects of fibre orientation from 0° to 90° will be illustrated

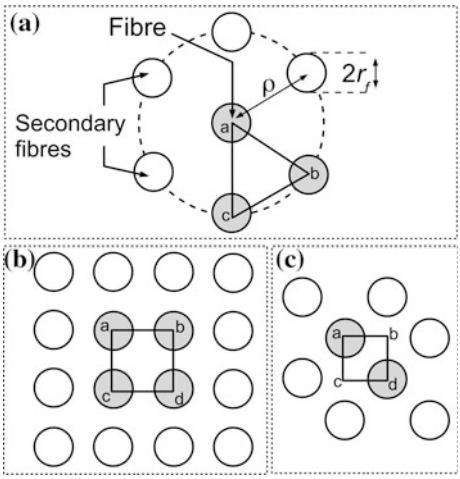

Fig. 2.9 Fibre arrangement in the matrix. **a** Hexagonal (triangular-edge) packing configuration. **b** Square-edge packing configuration. **c** Square-diagonal packing configuration. *Shaded circles* indicate the (primary) fibres of interest. Symbol r_f denotes radius, ρ denotes fibre–fibre separation distance

Similar arguments may be established for the other regular configurations For hexagonal (a.k.a triangular-edge) packing (Fig. 2.9a), there are three fibres in the region indicated by abc; the region has an area of $[3\sqrt{3}/2]\rho^2$. The total area of the fibre cross sections are given by $3\pi r_f^2$. One finds that $V_f = \{3\pi r_f^2 L_f\}/\{[3(\sqrt{3})/2]\rho^2 L_f\}$, which simplifies to [30, 71]

$$V_f = \{2\pi/\sqrt{3}\} r_f^2/\rho^2. \tag{2.16}$$

In general, V_f is related to r_f/ρ as follows [30],

$$V_f = w_f r_f^2/\rho^2, \tag{2.17}$$

where w_f is constant known as the packing factor. Thus, V_f increases with decreasing ρ and vice versa.

In particular, the values of w_f are defined as follows [30]:

- for square-edge packing (Fig. 2.9b), $w_f = \pi/2$;
- for square-diagonal packing (Fig. 2.9c), $w_f = \pi$;
- for hexagonal (a.k.a. triangular-edge) packing (Fig. 2.9a), $w_f = 2\pi/\{\sqrt{3}\}$.

For a detailed discussion of the derivation of these expressions see Piggott [71].

Equation (2.17) may be rewritten to take on a more general form that models the relationship between the (dimensionless) structural properties at composite level (i.e. V_f) and particle level (i.e. $S = \rho/r_f$, where $r_f = r_o$ for uniform cylindrical fibre) as follows:

$$V_f = w_f S^{-2}. \tag{2.18}$$

Figure 2.10 shows the graph of V_f versus S for the three different fibre packing configurations. In all cases, V_f decreases nonlinearly with increasing S. Of note, $S = 1$ corresponds to the situation where the fibre comes into contact with another fibre; no useful predictions can be determined from Eq. (2.18) for the case when $S > 1$. As shown in Fig. 2.10, the magnitude of V_f for the hexagonal packing is always larger than that of the square-diagonal and square-edge packing, for a given value of S.

Equation (2.18) presents an important structure-related length scale argument for DFRCs that addresses the link between the structural parameter at the fibre level to that at the composite level. Since Eq. (2.18) deals with dimensionless quantities, it suggests that the concept of scalability applies here. Thus, numerically, for a pre-determined V_f, Eq. (2.18) would always be satisfied even if ρ and r_f are defined with magnitudes of the order of metres (such as, huge steel rods embedded in concrete) or micrometres (such as whiskers reinforcing resin composites). Here, one

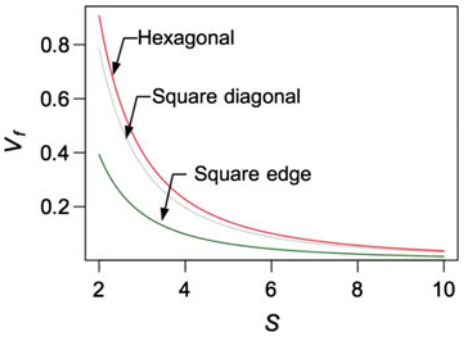

Fig. 2.10 Graph of fibre volume fraction, V_f, versus the fibre–fibre separation ratio, S, for hexagonal (a.k.a. triangular-edge), square-diagonal and square-edge packing configurations

should note that the concept of scalability could have a limitation [31]. In the macroscopic length scale, the deformation of most materials may be described by simple linear equations; a material undergoing small strain is often considered to behave linearly with regards to the force–displacement relationship. However, at the microscopic length scale, the same argument may not necessarily apply. For instance, silicon single crystal, which is a choice for the electronic industry, can easily undergo large strain, as compared to a beam made from a similar material [31]. For DFRCs, it may also be argued that the nanoclay silicon-based particles for reinforcing a composite [17, 18] is capable of undergoing high strain than would be expected of the same material at the macroscopic length scale.

2.4 Mechanical Properties

2.4.1 Composite Stiffness

Consider the DFRC described in Sect. 2.3.1. During the initial loading stage, the stress–strain curve is somewhat linear (Fig. 2.1). If strong adhesion exists between the fibres and the matrix, it follows that the overall strain experiences by the DFRC reflects the relative displacement between the fibres, regulated by the shear deformation of the interfibre matrix material. In this case, the elastic modulus of the DFRC, E, parameterizes the rate of change of stress uptake in the fibre with respect to the strain, which is predominantly contributed by the matrix.

An expression for E (Eq. 2.12) has been established based on the arguments used in the load-sharing concept (Sect. 2.3.3). Equation (2.12) is commonly referred to as the rule of mixture for the stiffness of the DFRC [1]. According to Eq. (2.12), the structural parameters of the fibre and matrix are, respectively, V_f and V_m while the material properties are E_f and E_m. Thus, E is regulated by the respective material properties and structure of the fibre and matrix. Several different expressions of the rule of mixtures for stiffness have been reported elsewhere [32–36]. In some reports, Eq. (2.12) is written with the term '$\beta_E E_f V_f$' in placed of $E_f V_f$, i.e.

$$E = \beta_E E_f V_f + E_m V_m, \tag{2.19}$$

where β_E represents a fibre efficiency factor ($\in [0,1]$) to account for the length of the fibre (Sect. 2.3) and/or the orientation of the fibre (Sect. 2.3.4) [8, 37]. Setting $\beta_E = 1$ in Eq. (2.19) gives

$$E = E_f V_f + E_m V_m, \tag{2.20}$$

which is identical to Eq. (2.12). The expression of E in Eq. (2.20) is often identified with the upper limit to the stiffness of the DFRC [1, 2]. With regards to the efficiency of reinforcement arising from fibre orientation, one finds $\beta_E \sim \eta$; the case of $\beta_E = 1$ applies when all the fibres are aligned in the direction of the applied

load. As previously indicated in Sect. 2.3.1, in this book, the fibres are always assumed to be aligned, in parallel, to the loading direction. Hereafter, unless otherwise stated, all discussions related to Eq. (2.19) are concerned with $\beta_E = 1$. Indeed, one may argue that since the fibres are aligned in the direction of the applied load, if E_f is a few orders of magnitudes higher than E_m, the property of E would be dominated by $E_f V_f$, valid to order of magnitude [2, 71]. This predominance is expected to increase with increasing V_f. However, there exists a critical V_f beyond which the E decreases with V_f. This is noted in Sect. 7.2.3 with regards to the other variant expressions of E (Eqs. 7.6 and 7.8).

Figure 2.11 shows a graph of the E versus V_f of discontinuous glass fibre reinforcing polypropylene composites. The graph compares the predictions from FE analysis of a 3D RVE (featuring randomly arranged discontinuous fibres) with data obtained by experiment [26]. The predictions reveal that the E increases as V_f increases, suggesting that the stiffening of the composite is contributed by the fibres oriented in the direction of the applied load. To some extent, this study shows that predictions from the RVE model [26] can lend support to the E versus V_f results of Kelly and Tyson [5]. However, as highlighted in previous paragraph with regards to the critical V_f, Thomason and Vlug [38] noted that high V_f (> 0.2), particularly for longer fibres, could result in fibre packing problems. Consequently, this increases the void spaces and E decreases with V_f (for further discussion on this issue see Sect. 7.2.3). On the other hand, fibre-like nanoparticles, such as halloysite nanotubes [39–42] and hydroxyapatites [6, 81], could lead to aggregation when blended into the matrix [78] and this could result in the diminution of the mechanical properties of the DFRC at high V_f (Sect. 7.2.3).

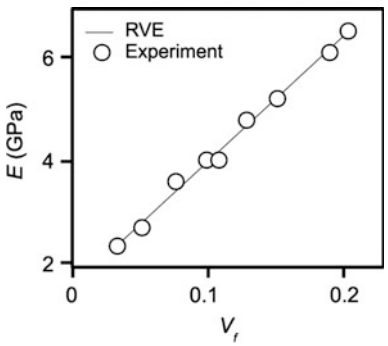

Fig. 2.11 Graph of the stiffness, E, of the DFRC versus fibre volume fraction, V_f, derived for discontinuous glass fibre reinforcing polypropylene matrix composites. The *line* represents predictions from finite element (FE) analysis [26]; *circles* represent results from experiment [38]. The graph is adapted from Lu et al. [26]. The FE analysis evaluated a representative volume element (RVE) of the glass–polypropylene matrix composite [26]; the experimental study was carried out using glass fibres (3-mm length) embedded in polypropylene matrix [38]. Key material parameters used for evaluating the RVE: fibre stiffness $E_f = 75$ GPa; matrix stiffness $E_m = 1.6$ GPa; Poisson's ratio of fibre $\nu_f = 0.25$; Poisson's ratio of matrix $\nu_m = 0.35$; shear modulus of fibre $G_f = 30$ GPa; shear modulus of matrix $G_m = 0.6$ GPa; fibre radius $r_o = 6.7$ μm

2.4.2 Composite Fracture Strength

An expression for the fracture strength, σ_U, of a DFRC may be estimated from the approach used in explaining the load-sharing concept (Eq. 2.8). Assuming that the fracture strain of the fibre and the matrix are of similar order of magnitude as the fracture strain of the DFRC, by substituting $E = \sigma_U/\varepsilon_U$, $E_f = \sigma_{f,U}/\varepsilon_{f,U}$ and $E_m = \sigma_{m,U}/\varepsilon_{m,U}$ into Eq. (2.12), this gives $\sigma_U \approx \sigma_{f,U}V_f + \sigma_{m,U}V_m$. This is the rule of mixture for composite fracture strength. It must be highlighted that the resulting expression then takes on an exact equality for the case of CFRC, i.e. $\sigma_U = \sigma_{f,U}V_f + \sigma_{m,U}V_m$. In general, the fracture strain of the fibre is lesser than that of the matrix, but $\sigma_{f,U}V_f \gg \sigma_{m,U}V_m$. To satisfy these constraints, this leads to an expression for the σ_U of a DFRC given by

$$\sigma_U = \beta_s \sigma_{f,U} V_f + \sigma_m V_m, \tag{2.21}$$

where σ_m is the average stress in the matrix at the fracture strain of the fibre (σ_m is considerably smaller than $\sigma_{f,U}$) and β_s is the fibre efficiency factor ($\in [0,1]$) for the DFRC fracture strength [3, 8]. Similar to the arguments that have been presented for β_E (Sect. 2.4.1), here the β_s is also related to the fibre length (Sect. 2.3.2) and fibre orientation (Sect. 2.3.4). Of note, other variants of the expression for the rule of mixtures for the composite fracture strength that depart from these simple expressions have been reported [2, 43–46].

As previously indicated in Sect. 2.3.1, the fibres are always preferentially aligned, in the direction of the applied load (Sect. 2.4.1). Thus, only the fibre length would affect the β_s. A full analysis of β_s is out of the scope of the book. Since this book is concerned with discontinuous fibres, it is important to note that the dependence of β_s on L_f (or q, if r_o is constant for all fibres) is more significant than that of continuous fibres [47]. It must also be emphasized that β_s is different from β_E (in fact, $\beta_s < \beta_E$). This is because the measure of σ_U involves subjecting the fibres in the DFRC to maximal stress uptake so that the magnitude of the maximum stress depends significantly on the q [3]. On the other hand, the E is a measure of the property of the DFRC at low strains and this does not significantly involve q [3].

One then finds that an upper bound of the fracture strength of the DFRC is given by setting $\beta_s = 1$. The expression for σ_U becomes

$$\sigma_U = \sigma_{f,U} V_f + \sigma_m V_m, \tag{2.22}$$

which has been widely reported elsewhere [3, 8]. For simplicity, all arguments presented hereafter that involves the rule of mixture for composite fracture strength will refer to the upper bound estimate of σ_U given by Eq. (2.22). (Of note, the DFRC models associated with the upper bounds for fracture strength (Eq. 2.22) and stiffness (Eq. 2.20) may be regarded as equivalent to the respective fracture strength and stiffness of CFRCs-these equations are often employed for CFRC design [82–84].)

Figure 2.12a and b shows graphs of σ_U versus V_f, for different q values derived from experiments carried out on tungsten fibres reinforcing copper composites [5]

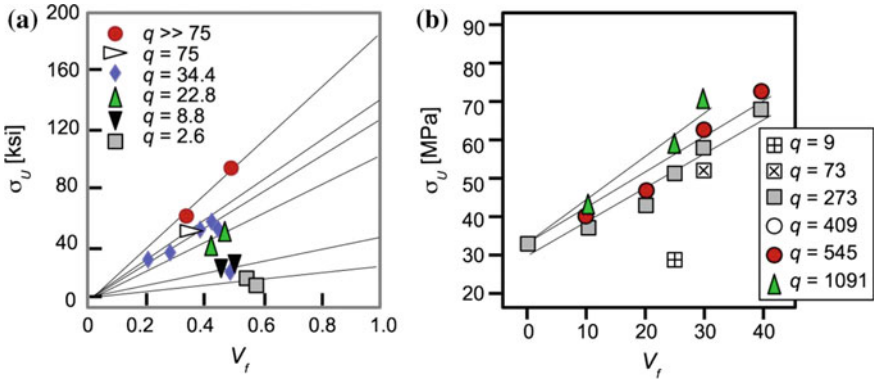

Fig. 2.12 Graphs of the DFRC fracture strength, σ_U, versus the fibre volume fraction, V_f, for **a** tungsten fibres reinforcing copper composites [5] and **b** glass fibres reinforcing polypropylene matrix composites [48]

and glass fibres reinforcing polypropylene matrix composites, respectively [48]. In both cases, σ_U increases with increasing V_f. Also, the higher the q value, the steeper is the gradient of the σ_U versus V_f. In both cases, apart from the results at low qs, it is observed that the experimental data points from the respective qs appear to be in good agreement with the predictions derived from Eq. (2.22), suggesting that σ_U increases linearly with increasing V_f.

In case of the yield strength of the DFRC, σ_Y, one may describe the upper bound of σ_Y in terms of the $\sigma_{f,Y}$, σ_m and V_f by borrowing an argument relating to dislocation mechanisms in a polycrystalline material containing two physically dissimilar phases [49]. On the basis of this argument [49], it follows that the DFRC undergoes yielding when $\sigma_Y \approx \sigma_{f,Y}V_f + \sigma_m V_f$ where $\sigma_{f,Y}$ refers to the yield strength of the fibre and σ_m (in this case) is simply the average stress in the matrix at the yield stress of the fibre.

2.4.3 *Resilience and Fracture Toughness*

Owing to the variability in the manufacturing process for the fibres, the size of the fibre, such as fibre diameter, D_f, would also vary [50]. The purpose of this section is to present arguments to connect the frequency distribution of D_f with the respective strain energy density for resilience (u_Y) and fracture toughness (u_C) of the DFRC.

To begin, suppose the DFRC comprises n_D populations of fibres, distinguished by the respective mean D_fs. For simplicity, the relationship between the mean D_fs and the respective u_Y and u_C can be expressed as follows:

$$u_Y/\sigma_Y = \sum_i c_{E,i} D_{f,i}, \tag{2.23}$$

and

$$u_C/\sigma_U = \sum_i c_{RP,i} D_{f,i} \tag{2.24}$$

[51], where $i = 1, 2, \ldots n_D$, and $D_{f,i}$ denotes the mean D_f of the ith distribution, The $c_{E,i}$ and $c_{RP,i}$ are constants of proportionality. The $c_{E,i}$ is expressed in terms of the mechanical properties of the fibre (namely $\sigma_{f,Y}$ and E_f), the fibre–matrix interfacial parameter (namely τ), and a scale factor for length. The $c_{RP,i}$ is given by

$$c_{RP,i} = c_{R,i} + c_{P,i}, \tag{2.25}$$

where, c_{R1} and c_{R2} are expressed in terms of the mechanical properties of the fibre (namely $\sigma_{f,U}$ and E_f), the fibre–matrix interfacial parameter (namely τ) and a scale factor for length. Thus, Eqs. (2.23–2.25) provide a method for estimating the strain energies absorbed for resilience and fracture toughness, in terms of the mean fibre diameter of the respective fibre distribution in the DFRC.

In particular, $n_D = 2$ is identified with a population of fibres characterized by a bimodal distribution of fibre diameters. For the purpose of illustration, Fig. 2.13 shows a histogram of frequency versus fibre diameter for a hypothetical DFRC with a bimodal fibre diameter distribution. Here, each distribution follows the characteristics of a normal distribution—the combination of the two distributions results in a distribution which appears to be slightly skewed to the left.

According to Goh and coworkers [51], for the DFRC, Eqs. (2.23–2.25) become,

$$u_Y/\sigma_Y = c_{E,1} D_{f,1} + c_{E,2} D_{f,2}, \tag{2.26}$$

$$u_C/\sigma_U = c_{RP,1} D_{f,1} + c_{RP,2} D_{f,2}, \tag{2.27}$$

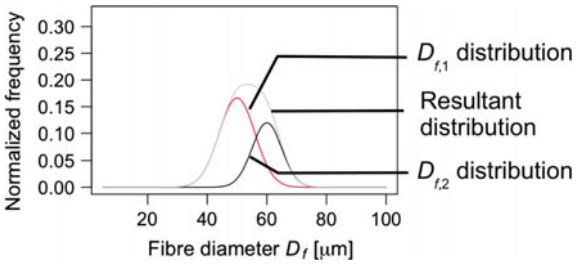

Fig. 2.13 Histogram of frequency versus fibre diameter, D_f. Here the *red* and *black lines* represent the fibre populations corresponding to mean fibre diameters $D_{f,1} = 50$ and $D_{f,2} = 60$ (SD = 5 in both cases), respectively. The resultant distribution is derived by summing the two distributions. The values for the fibre mean diameter and standard deviation quoted here are for illustrative purposes

where c_{RP1} and c_{RP2} are

$$c_{RP,1} = c_{R,1} + c_{P,1}, \tag{2.28}$$

$$c_{RP,2} = c_{R,2} + c_{P,2}. \tag{2.29}$$

These relationships, namely Eqs. (2.26) and (2.27), provide a practical approach to incorporate the fibre diameter in the analysis of the mechanical reliability of the DFRC. The formulation of these relationships, including the complementary equations, Eqs. (2.28) and (2.29), addresses the contribution of the mechanisms of fibre–matrix debonding (Sect. 4.3.3), matrix crack initiation (Sect. 4.3.4), plastic stress transfer (Sect. 5.3), matrix fracture (Sect. 6.2.1), fibre pull-out (Sect. 6.2.2) and fibre fracture (Sect. 6.2.3) to the respective u_Y and u_C. Of note, these relationships were first applied to study the effects of the fibre diameter on the resilience and fracture toughness of collagen fibre reinforced connective tissues [51], which are biological examples of DFRC [74–75, 85–86, 89–91]. The D_f is an important structural parameter because it is related to q (Eq. 2.1). Here, the D_f is presented as an important parameter for influencing u_Y and u_C but the significance of this may be realized further by considering the predictions from these models of u_Y and u_C together with the Griffith's critical crack length arguments for evaluating how an initial microcrack propagates across the fibre cross section (Sect. 1.4).

How can one measure the diameters of fibres in composites in situ? One way is to employ a non-destructive test apparatus such as X-ray computed tomography (CT). X-ray CT is ideal as an inspection tool for composite testing because it can reveal the internal structure of the composite, including defects [52], by generating a 3D volumetric representation of the scanned composite specimen, based on a reconstruction approach from a series of 2D projection X-ray images taken through a complete rotation of the specimen [53, 54]. Thereafter, one can perform image analysis to quantify the fibre diameter. Currently, X-ray CT systems can produce images with voxel sizes of 500 nm; this allows for generating high resolution images for the analysis of the structure of fibres at the nanometre and micrometre length scales [53]. However, not all materials can be imaged successfully. Some materials, namely metals, could degrade the radiographic contrast as well as produce artefacts in the X-ray CT images owing to the high X-ray absorption properties [55]. One way to solve this is to use the dual energy X-ray CT method [54–56]. Dual energy X-ray CT devices apply the concept of material decomposition [57, 58] to enable both fibre and matrix components in the composite to be distinguished by requiring that the imaging of the composite be performed at two different X-ray (spectral) energies [57, 58]. This works for as long as the fibre and matrix components are endowed with X-ray attenuation properties that lie in between those of the calibration materials [54–58]. Of note, the conventional X-ray CT device uses only one X-ray (spectral) energy. Dual energy X-ray CT devices can also image components with low attenuation properties that are located adjacent to high attenuation ones, which is not always possible with the conventional X-ray

CT approach [55]. A full account of the use of CT devices for examining composites would be far beyond the scope of this book. The interested reader is referred to the literature cited in this paragraph for further details.

2.4.4 Probabilistic Analysis of Fracture

In ceramics, the presence of imperfections can contribute to the low fracture toughness of the material. Even moulded polymer components often contain defects such as small microscopic voids or cracks [10–13]. For fibre-like nanoparticles such as carbon nanotubes, the presence of Stone-Wales defects can dramatically influence the energy absorbed by the nanotube when it is loaded in tension [79] or in torsion [80]. As pointed out in Sect. 1.6, this effect could compromise the strength of the nanotube. These materials are likely to fail by fracture (before they can even yield) at the sites of the defect. These voids or crack-related defects can also occur during the manufacturing process. Thereafter, how the crack-related defects propagate across the fibre cross section depends on the size of the crack, which is parameterized by c_0; this has been discussed in Sect. 1.4. Not surprising, the strength of such materials will vary because of the variability in the c_0 (or b_0). When using brittle materials for making fibres to provide reinforcement to a composite, if the composite is subjected to a service load, one may not always be certained that the fibres will not fail. A practical solution in engineering is to adopt an acceptable risk (the failure probability) for the function that is to be performed by the composite and design the composite so that this acceptable risk is met [59]. Since fracture toughness is modelled in terms of the fracture strength of the material in many theories of fracture mechanics, thus it is important to develop the design arguments for an acceptable risk from the perspective of fracture strength.

The probability density function, P_{PDF}, with respect to $\sigma_{\mathrm{f,U}}$ may be modelled by a Weibull distribution, i.e. $P_{\mathrm{PDF}} = m[\sigma/\sigma_{\mathrm{f,U}}]^{m-1}\exp(-\{\sigma/\sigma_{\mathrm{f,U}}\}^m)$, where m is known as the 'Weibull modulus' of the (Weibull) distribution, σ may be identified with the applied stress acting on the material [47, 60] and $\sigma_{\mathrm{f,U}}$ is regarded as the characteristic strength of the fibre [61, 62]. The shape of the plot of this function, i.e. P_{PDF} versus σ, varies drastically with m. When $m = 0.5$ the function features a Lorentzian-like profile, but this takes on a profile resembling a chi-square distribution at $m = 2$ and a near-normal distribution at $m = 5$. For this reason, a more convenient expression is the associated cumulative distribution function given by

$$P_{\mathrm{Fail1}} = 1 - \exp(-[\sigma/\sigma_{\mathrm{f,U}}]^m), \tag{2.30}$$

where P_{Fail1} quantifies the proportion of fibres with a designated $\sigma_{\mathrm{f,U}}$, rupturing when subjected to a stress σ [34, 62, 63]. From a practical point of view, the P_{Fail1} distribution is a more convenient model than the P_{PDF} because the profile of the plot of P_{Fail} versus σ is not as wildly sensitive to m as P_{PDF}. With regard to Eq. (2.30), the m is now responsible for regulating the spread of the profile. Figure 2.14a

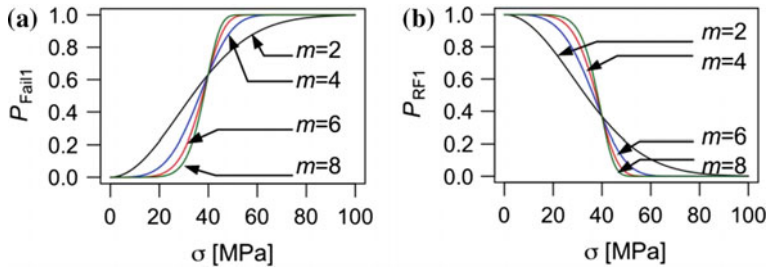

Fig. 2.14 Probabilistic analysis. **a** Graph of cumulative probability distribution, P_{Fail1}, versus the applied stress on the DFRC, σ. **b** Graph of survival probability (a.k.a. the reliability function), P_{RF1}, versus σ. In both graphs, the results are obtained by evaluating the respective models given by Eqs. (2.30) and (2.31), where the characteristic fracture strength of the fibre, $\sigma_{f,U}$, is set at 40 MPa. Here the Weibull modulus, m = 2, 4, 6 and 8. All input values assigned to this example are for the purpose of illustration

shows the graph of the P_{Fail1} versus the σ for different values of m. The lower the value of m, the greater the variability of strength; the higher the value of m, the smaller the variability of strength.

What does the P_{Fail1} say about the failure (i.e. fracture) of a fibre? When $\sigma = 0$, all the fibres will survive, and $P_{Fail1} = 0$. As σ increases, the number of fibres failing increases, and P_{Fail1} increases. Very large σ (i.e. $\sigma \to \infty$) could cause all the fibres to break, so $P_{Fail1} = 1$. When $\sigma = \sigma_{f,U}$, this results in $P_{Fail1} = 1 - 1/e = 0.63$. In other words, $\sigma_{f,U}$ is the stress that could result in 63 % of the fibres to fail.

Another way of approaching the analysis of fibre failure is to define the surviving probability, P_{RF1} (= $1 - P_{Fail1}$), or otherwise known as the reliability function [64]. Thus,

$$P_{RF1} = \exp(-[\sigma/\sigma_{f,U}]^m). \tag{2.31}$$

Figure 2.14b shows the graph of the P_{RF1} versus the σ for different values of m. When $\sigma = 0$, all the fibres will survive and $P_{RF1} = 1$. As σ increases, the number of fibres failing increases, and P_{RF1} decreases. Very large σ (i.e. $\sigma \to \infty$) could cause all the fibres to break, so $P_{RF1} = 0$. When $\sigma = \sigma_{f,U}$, this results in $P_{RF1} = 1/e = 0.37$. In other words, $\sigma_{f,U}$ is the stress that could result in 37 % of the fibres to survive.

Equations (2.30) and (2.31) describe the stress dependence of P_{Fail1} and P_{RF1} but the analysis only takes into account the mechanical behaviour governing a single fibre. For the analysis of the strength of a bundle of fibres (in the absence of the matrix [65] or in the presence of a matrix [66]), these equations will have to account for the number of fibres present. It is more useful to be able to predict the fibre bundle system because this would indicate to the designer the reliability of the composite material when it is used to build structures. Let V_0 be the volume of a single fibre. It follows that the probability that a bundle of N fibres stuck together to give a total volume V, all survive a stress σ is $P_{RF} = \{P_{RF1}\}^N$ [64]. Thus, P_{RF} may be written as follows [64]:

$$P_{RF} = \exp(-N[\sigma/\sigma_{f,U}]^m), \tag{2.32}$$

or

$$P_{RF} = \exp(-\{V/V_0\}[\sigma/\sigma_{f,U}]^m). \tag{2.33}$$

Note that Eqs. (2.32) and (2.33) assume that the bundle of fibres is subjected to a uniform stress σ. In DFRCs, for a given applied load acting on the DFRC, the fibres may not necessarily be experiencing the same stress. However, if one assumes that (1) the fibres are present in a sufficiently large number and (2) the fibres are aligned, so that the NA_f/A_c at a given cross section of the DFRC is constant, as indicated previously in Sect. 2.3.1, from a statistical perspective, then it is possible to apply the Eqs. (2.32) and (2.33) to such an assembly of discontinuous fibres in the DFRC [67]. Further discussion is found in Sect. 6.2.5.

Also, note that in some reports, the argument in the exponent of Eq. (2.30) is written as '$-[\{\sigma - \sigma'\}/\sigma_{f,U}]^m$' where σ' is a threshold stress below which one may assumed that the fibre has zero probability of fracture [68]. For simplicity, σ' is set to zero since the Weibull distribution with $\sigma' = 0$ will lead to the least-biased results [69].

How does one apply the Weibull distribution for probabilistic strength analysis? A typical approach is presented as follows for P_{Fail} [7]. To begin, the P_{Fail} is identified with the median rank (MR), which is expressed as [7, 81]

$$\text{MR} = \{i - 0.3\}/\left[n_{spec} + 0.4\right], \tag{2.34}$$

where i is the rank of fibre fracture strength value in ascending order, and n_{spec} is the total number of specimens tested [7]. Next, one applies the double logarithm on both sides of the Eq. (2.30) as follows

$$\log_e(-\log_e(1 - P_{Fail})) = m\log_e(\sigma) - m\log_e(\sigma_{f,U}). \tag{2.35}$$

Then one fits the Eq. (2.35) to the experimental data using linear regression analysis by plotting a graph of $\log_e(-\log_e(1 - P_{Fail}))$ versus $\log_e(\sigma))$ [7, 81]. This enables the slope, i.e. m, of the fitted straight line to be determined. By identifying $m\log_e\sigma_{f,U}$ with the value of the y-intercept, this enables the magnitude of $\sigma_{f,U}$ to be predicted.

The Weibull distribution has broad applications. As shown in previous reports, it can be applied to the analysis of any design factor which features variability (resulting in a distribution pattern when measurements are taken), e.g. yield strength of the fibres, size (diameter) of the fibres [61] and even fibre length [34, 70].

2.5 Summary

The stress versus strain curve of a DFRC reveals a variety of underlying mechanisms involve in regulating the ability of the fibres to provide reinforcement to the matrix until the composite material ruptures. These mechanisms may be broadly categorized as stress transfer and fracture mechanisms. As a two-phase material, the fibre and matrix interact to enable the load to be taken up by the composite and to be shared between the two phases. The extent of the load sharing capability depends on the volume fraction of the respective phases. The packing configuration of the fibres influences the V_f; among the three regular packing configurations, namely hexagonal, square diagonal and square edge, the hexagonal packing and square edge configurations always give the highest and lowest V_f, respectively. The q, which is a measure of the slenderness of a fibre, is an important structural parameter because it influences the key mechanical properties of a DFRC. It turns out that high slenderness leads to augmentation of several key mechanical properties, namely E, σ_Y, σ_U, ε_Y, ε_U, u_Y and u_C. Both the E and σ_U can be predicted to some certainty if the corresponding mechanical properties of the respective fibre and matrix are known, for a given V_f. The q influences the u_Y and u_C through the D_f. Probabilistic analysis, using the Weibull distribution as the basis of evaluation, can incorporate the variability arising from defects present in the fibres to make useful predictions about the variability of the fracture strength of the fibres in the DFRC.

References

1. Agarwal BD, Broutman LJ, Chandrashekhara K. Analysis and performance of fiber composites. 3rd ed. New Jersey: Wiley; 2006.
2. Kelly A, Macmillan NH. Strong solids. 3rd ed. Oxford: Oxford University Press; 1986.
3. Fu SY, Lauke B, Mäder E, Yue CY, Hu X. Tensile properties of short-glass-fiber- and short-carbon-fiber-reinforced polypropylene composites. Compos A Appl Sci Manuf. 2000;31:1117–25.
4. Blassiau S, Thionnet A, Bunsell AR. Micromechanisms of load transfer in a unidirectional carbon fibre-reinforced epoxy composite due to fibre failures: Part 3. Multiscale reconstruction of composite behaviour. Compos Struct. 2008;83:312–23.
5. Kelly A, Tyson WR. Tensile properties of fibre-reinforced metals: copper/tungsten and copper/molybdenum. J Mech Phys Soilds. 1965;13:329–50.
6. Xie JZ, Hein S, Wang K, Liao K, Goh KL. Influence of hydroxyapatite crystallization temperature and concentration on stress transfer in wet-spun nanohydroxyapatite–chitosan composite fibres. Biomed Mater. 2008;3:2–6.
7. Chew SL, Wang K, Chai SP, Goh KL. Elasticity, thermal stability and bioactivity of polyhedral oligomeric silsesquioxanes reinforced chitosan-based microfibres. J Mater Sci Mater Med. 2011;22:1365–74.
8. Fu SY, Feng XQ, Lauke B, Mai YW. Effects of particle size, particle/matrix interface adhesion and particle loading on mechanical properties of particulate-polymer composites. Compos B Eng. 2008;39:933–61.
9. Ehrburger P, Donnet JB. Interface in composite materials. Philos Trans R Soc A Math Phys Eng Sci. 1980;294:495–505.

10. Tan LP, Joshi SC, Yue CY, Lam YC, Hu X, Tam KC. Effect of shear heating during injection molding on the morphology of PC/LCP blends. Acta Mater. 2003;51:6269–76.
11. Tan LP, Yue CY, Tam KC, Lam YC, Hu X, Nakayama K. Relaxation of liquid-crystalline polymer fibers in polycarbonate–liquid-crystalline polymer blend system. J Polym Sci B Polym Phys. 2003;41:2307–12.
12. Tan LP, Yue CY, Tam KC, Lam YC, Hu X. Effect of compatibilization in injection-molded polycarbonate and liquid crystalline polymer blend. J Appl Polym Sci. 2002;84:568–75.
13. Tan LP, Yue CY, Tam KC, Lam YC, Hu X. Effects of shear rate, viscosity ratio and liquid crystalline polymer content on morphological and mechanical properties of polycarbonate and LCP blends. Polym Int. 2002;51:398–405.
14. Goh KL, Aspden RM, Mathias KJ, Hukins DWL. Effect of fibre shape on the stresses within fibres in fibre-reinforced composite materials. Proc R Soc Lond A. 1999;455:3351–61.
15. Goh KL, Mathias KJ, Aspden RM, Hukins DWL. Finite element analysis of the effect of fibre shape on stresses in an elastic fibre surrounded. J Mater Sci. 2000;5:2493–7.
16. Goh KL, Huq AMA, Aspden RM, Hukins DWL. Nano-fibre critical length depends on shape. Adv Compos Lett. 2008;17:131–3.
17. Wang HW, Zhou HW, Peng RD, Mishnaevsky L. Nanoreinforced polymer composites: 3D FEM modeling with effective interface concept. Compos Sci Technol. 2011;71:980–8.
18. Liu H, Brinson LC. Reinforcing efficiency of nanoparticles: a simple comparison for polymer nanocomposites. Compos Sci Technol. 2008;68:1502–12.
19. Mortazavi B, Baniassadi M, Bardon J, Ahzi S. Modeling of two-phase random composite materials by finite element, Mori–Tanaka and strong contrast methods. Compos B. 2013;45:1117–25.
20. Lin TH, Salinas D, Ito YM. Elastic–plastic analysis of unidirectional composites. J Compos Mater. 1972;6:48–60.
21. Kelly A. Interface effects and the work of fracture of a fibrous composite. Proc R Soc Lond A. 1970;319:95–116.
22. Harris J, Bond IP, Weaver PM, Wisnom MR, Rezai A. Measuring strain energy release rate (GIc) in novel fibre shape composites. Compos Sci Technol. 2006;66:1239–47.
23. Pan N. The elastic constants of randomly oriented fiber composites: a new approach to prediction. Sci Eng Compos Mater. 1996;5:63–72.
24. Aspden RM. Fibre stress and strain in fibre-reinforced composites. J Mater Sci. 1994;29:1310–8.
25. Tian W, Qi L, Zhou J, Guan J. Effects of the fiber orientation and fiber aspect ratio on the tensile strength of Csf/ Mg composites. Comput Mater Sci. 2014;89:6–11.
26. Lu Z, Yuan Z, Liu Q. 3D numerical simulation for the elastic properties of random fiber composites with a wide range of fiber aspect ratios. Comput Mater Sci. 2014;90:123–9.
27. Xiao T, Ren Y, Liao K, Wu P, Li F, Cheng HM. Determination of tensile strength distribution of nanotubes from testing of nanotube bundles. Compos Sci Technol. 2008;68:2937–42.
28. Newcomb BA, Gi H, Gulgunje PV, Gupta K, Liu Y, Tsentalovich DE, et al. Stress transfer in polyacrylonitrile/carbon nanotube composite fibers. Polymer. 2014;55:2734–43.
29. Mortazavian S, Fatemi A. Effects of fiber orientation and anisotropy on tensile strength and elastic modulus of short fiber reinforced polymer composites. Compos B. 2015;72:116–29.
30. Mohonee VK, Goh KL. Effects of fibre–fibre interaction on stress uptake in discontinuous fibre reinforced composites. Compos B Eng. 2016;86:221–8.
31. Ward MCL. Concepts in nanomechanics. Nanotechnol Percept. 2008;4:239–46.
32. Tucker CL, Liang E. Stiffness predictions for unidirectional short-fiber composites: Review and evaluation. Compos Sci Technol. 1999;59:655–71.
33. Torquato S. Modeling of physical properties of composite materials. Int J Solids Struct. 2000;37:411–22.
34. Robinson IM, Robinson JM. The influence of fibre aspect ratio on the deformation of discontinuous fibre-reinforced composites. J Mater Sci. 1994;29:4663–77.

35. Lopez JP, Mutje P, Pelach MA, El Mansouri N-E, Boufi S, Vilaseca F. Analysis of the tensile modulus of polypropylene composites reinforced with stone groundwood fibers. BioResources. 2012;7:1310–23.
36. Liang J-Z. Predictions of Young's modulus of short inorganic fiber reinforced polymer composites. Compos B Eng. 2012;43:1763–6.
37. Zeng QH, Yu AB, Lu GQ. Multiscale modeling and simulation of polymer nanocomposites. Prog Polym Sci. 2008;33:191–269.
38. Thomason JL, Vlug MA. Influence of fibre length and concentration on the properties of glass fibre-reinforced polypropylene: 1. Tensile and flexural modulus. Compos A. 1996;27A:477–84.
39. De Silva RT, Soheilmoghaddam M, Goh KL, Wahit MU, Abd Bee, Hamid S, Chai S-P, et al. Influence of the processing methods on the properties of poly (lactic acid)/halloysite nanocomposites. Polym Compos. 2016;37:861–69.
40. De Silva RT, Pasbakhsh P, Goh KL, Chai S-P, Ismail H. Physico-chemical characterisation of chitosan/halloysite composite membranes. Polym Test. 2013;32:265–71.
41. De Silva RT, Pasbakhsh P, Goh KL, Mishnaevsky L. 3-D computational model of poly (lactic acid)/halloysite nanocomposites: predicting elastic properties and stress analysis. Polymer. 2014;55:6418–25.
42. De Silva RT, Pasbakhsh P, Goh KL, Chai S-P, Chen J. Synthesis and characterisation of poly (lactic acid)/halloysite bionanocomposite films. J Compos Mater. 2014;48:3705–17.
43. Andersons J, Sparnins E, Joffe R. Stiffness and strength of flax fiber/polymer matrix composites. Polym Compos. 2006;27:221–9.
44. Okabe T, Sasayama T, Koyanagi J. Micromechanical simulation of tensile failure of discontinuous fiber-reinforced polymer matrix composites using spring element model. Compos A. 2014;56:64–71.
45. Petersen RC, Lemons JE, Mccracken MS. Stress-transfer micromechanics for fiber length with a photocure vinyl ester composite. Polym Compos. 2006;27:153–69.
46. Piggott MR. Expressions governing stress–strain curves in short fibre reinforced polymers. J Mater Sci. 1978;13:1708–16.
47. Fu S, Lauke B. Effects of fiber length and fiber orientation distributions on the tensile strength of short-fiber-reinforced polymers. Compos Sci Technol. 1996;56:1179–90.
48. Thomason JL, Vlug MA, Schipper G. Krikor HGLT. Influence of fibre length and concentration on the properties of glass fibre-reinforced polypropylene: Part 3. Strength and strain at failure. Compos A Appl Sci Manuf. 1996;27:1075–84.
49. Dai CY, Xu J, Zhang B, Zhang GP. Understanding scale-dependent yield stress of metals at micrometre scales. Philos Mag Lett. 2013;93:531–40.
50. Heikkilä P, Harlin A. Electrospinning of polyacrylonitrile (PAN) solution: effect of conductive additive and filler on the process. Express Polym Lett. 2009;3:437–45.
51. Goh KL, Holmes DF, Lu Y, Purslow PP, Kadler KE, Bechet D, et al. Bimodal collagen fibril diameter distributions direct age-related variations in tendon resilience and resistance to rupture. J Appl Physiol. 2012;113:878–88.
52. Bliznakova K, Dermitzakis A, Bliznakov Z, Kamarianakis Z, Buliev I, Pallikarakis N. Modeling of small carbon fiber-reinforced polymers for X-ray imaging simulation. J Compos Mater. 2014;0:1–13.
53. Weissenböck J, Bhattacharya A, Plank B, Heinzl C, Kastner J. Visual classification of braided and woven fiber bundles in X-ray computed tomography scanned carbon fiber reinforced polymer specimens. Case Stud Nondestruct Test Eval. 2016;1:1–8.
54. Sause MGT. In situ monitoring of fiber-reinforced composites: theory, basic concepts, methods, and applications. Berlin: Springer; 2016.
55. Vavrik D, Jakubek J, Kumpova I, Pichotka M. Dual energy CT inspection of a carbon fibre reinforced plastic composite combined with metal components. Case Stud Nondestruct Test Eval. 2016; http://dx.doi.org/10.1016/j.csndt.2016.05.001.

56. Robert C, Dinten JM, Rizo P. Dual-energy computed tomography for ceramics and composite. In: Thompson DO, Chimenti DE, editors. Review of progress in quantitative nondestructive evaluation. New York: Plenum Press; 1996. p. 481–8.
57. Goh KL, Liew SC, Hasegawa BH. Energy-dependent systematic errors in dual-energy X-ray CT. IEEE Trans Nucl Sci. 1997;44:212–7.
58. Goh KL, Liew SC, Hasegawa BH. Correction of energy-dependent systematic errors in dual-energy X-ray CT using a basis material coefficeints transformation method. IEEE Trans Nucl Sci. 1997;44:2419–24.
59. Dobrza LA. Significance of materials science for the future development of societies. J Mater Process Technol. 2006;175:133–48.
60. Klein CA. Characteristic strength, Weibull modulus, and failure probability of fused silica glass. Opt Eng. 2009;48:113401.
61. Weibull W. A statistical distribution function of wide applicability. ASME J Appl Mech. 1951;18:293–7.
62. Wisnom MR, Green D. Tensile failure due to interaction between fibre breaks. Composites. 1995;26:499–508.
63. Naito K, Yang J-M, Kagaw Y. Tensile properties of high strength polyacrylonitrile (PAN)-based and high modulus pitch-based hybrid carbon fibers-reinforced epoxy matrix composite. J Mater Sci. 2012;47:2743–51.
64. Ashby MF, Jones DRH. Engineering Materials 1: an introduction to properties, applications, and design. 4th ed. Oxford: Elsevier Ltd; 2009.
65. Zussman E, Chen X, Ding W, Calabri L, Dikin DA, Quintana JP, et al. Mechanical and structural characterization of electrospun PAN-derived carbon nanofibers. Carbon N Y. 2005;43:2175–85.
66. Moser B, Weber L, Rossoll A, Mortensen A. The influence of non-linear elasticity on the determination of Weibull parameters using the fibre bundle tensile test. Compos A. 2003;34:907–12.
67. Rosen BW. Mechanics of composite strengthening. In: Fibre composite materials. Metals Park: American Society of Metals; 1965. p. 37–75.
68. Naito K, Tanaka Y, Yang J-M, Kagawa Y. Tensile properties of ultrahigh strength PAN-based, ultrahigh modulus pitch-based and high ductility pitch-based carbon fibers. Carbon N Y. 2008;46:189–95.
69. Trustrum K, Jayatilaka ADS. On estimating the Weibull modulus for a brittle material. J Mater Sci. 1979;14:1080–4.
70. Wimolkiatisak AS, Bell JP. Interfacial shear strength and failure modes of interphase-modified graphite-epoxy composites. Polym Compos. 1989;10:162–72.
71. Piggott M. Load bearing fibre composites. 2nd ed. Dordrecht: Kluwer; 2002.
72. Goh KL, Aspden RM, Mathias KJ, Hukins DWL. Finite-element analysis of the effect of material properties and fibre shape on stresses in an elastic fibre embedded in an elastic matrix in a fibre-composite material. Proc R Soc Lond A. 2004a;460:2339–52.
73. Goh KL, Aspden RM, Hukins DWL. Review: finite element analysis of stress transfer in short-fibre composite materials. Compos Sci Technol. 2004b;64:1091–100.
74. Goh KL, Aspden RM, Hukins DWL. Shear lag models for stress transfer from an elastic matrix to a fibre in a composite material, Int J Mater Struct Integrity. 2007;1(1–3):180–89.
75. Goh KL, Meakin JR, Hukins DWL. Influence of fibre taper on the interfacial shear stress in fibre-reinforced composite materials during elastic stress transfer. Compos Interfaces. 2010;17:75–1.
76. Goh KL, Huq AMA, Aspden RM, Hukins DWL. Nano-fibre critical length depends on shape. Adv Compos Lett. 2008;17:131–3.
77. Ng XW, Hukins DWL, Goh KL. Influence of fibre taper on the work of fibre pull-out in short fibre composite fracture. J Mater Sci. 2010;45:1086–90.
78. De Silva R, Pasbakhsh P, Qureshi AJ, Gibson AG, Goh KL. Stress transfer and fracture in nanostructured particulate-reinforced chitosan biopolymer composites: influence of interfacial shear stress and particle slenderness. Composite Interfaces, 2014;21(9):807–818.

79. Huq AMA, Goh KL, Zhou ZR, Liao K. On defect interactions in axially loaded single-walled carbon nanotubes. J Appl Phys. 2008;103:054306.
80. Huq AMA, Bhuiyan AK, Liao K, Goh KL. Defect-defect interaction in single-walled carbon nanotubes under torsional loading. Int J Mod Phys B. 2010;24:1215–26.
81. Wang K, Liao K, Goh KL. How sensitive is the elasticity of hydroxyapatite-nanoparticle-reinforced chitosan composite to changes in particle concentration and crystallization temperature? J Funct Biomater. 2015;6(4):986–98.
82. Herakovich CT. Mechanics of composites: A historical review. Mechanics Research Communications. 2012;4:11–20.
83. Buana SASM, Pasbaskhsh P, Goh KL, Bateni F, Haris MRHM. Elasticity, microstructure and thermal stability of foliage and fruit fibres from four tropical crops. Fibers Polym. 2013;14:623–9.
84. Fong TC, Saba N, Liew CK, De Silva R, Hoque ME, Goh KL. Yarn flax fibres for polymer-coated sutures and hand layup polymer composite laminates. In: Salit MS, Jawaid M, Yusoff NB, Hoque ME, editors. Manufacturing of natural fibre reinforced polymer composites. Berlin: Springer; 2015. p. 155–75.
85. Goh KL, Hukins DWL, Aspden RM. Critical length of collagen fibrils in extracellular matrix. J Theor Biol. 2003;223:259–61.
86. Goh KL, Meakin JR, Aspden RM, Hukins DWL. Influence of fibril taper on the function of collagen to reinforce extracellular matrix. Proc R SocB 2005;272:1979–83.
87. Goh KL, Meakin JR, Aspden RM, Hukins DWL. Stress transfer in collagen fibrils reinforcing connective tissues: Effects of collagen fibrilslenderness and relative stiffness. J Theor Biol. 2007;245:305–11.
88. Goh KL, Chen Y, Chou SM, Listrat A, Bechet D, Wess TJ. Effects of frozen storage temperature on the elasticity of tendons from a small murine model. Animal. 2010;4 (09):1613–17.
89. Goh KL, Listrat A, Bechet D. Hierarchical mechanics of connective tissues: Integrating insights from nano to macroscopic studies. J Biomed Nanotechnol. 2014a;10:2464–07.
90. Goh KL, Chen SY, Liao K, A thermomechanical framework for reconciling the effects of ultraviolet radiation exposure time and wavelength on connective tissue elasticity. Biomech Modell Mechanobiology, 2014b;13:1025–40.
91. Yeo YL, Goh KL, Liao K, Wang HJ, Listrat A, Bechet D. Structure-property relationship of burn collagen reinforcing musculo-skeletal tissues.Key Eng Mater. 2011;478:87–92.

http://www.springer.com/978-1-4471-7303-8

Discontinuous-Fibre Reinforced Composites
Fundamentals of Stress Transfer and Fracture Mechanics
Goh, K.L.
2017, XXIV, 190 p. 88 illus., Hardcover
ISBN: 978-1-4471-7303-8